

Emergence of memory manifolds

Tankut Can^{1,*} and Kamesh Krishnamurthy^{2,*}

¹*Initiative for Theoretical Sciences,
Graduate Center, CUNY, New York
and*

*School of Natural Sciences,
Institute for Advanced Study, Princeton NJ*

²*Joseph Henry Laboratories of Physics and PNI, Princeton University, Princeton NJ*

(Dated: March 14, 2022)

The ability to store continuous variables in the state of a biological system (e.g. a neural network) is critical for many behaviours. Most models for implementing such a memory manifold require hand-crafted symmetries in the interactions or precise fine-tuning of parameters. We present a general principle that we refer to as *frozen stabilisation*, which allows a family of neural networks to self-organise to a critical state exhibiting memory manifolds without parameter fine-tuning or symmetries. These memory manifolds exhibit a true continuum of memory states and can be used as general purpose integrators for inputs aligned with the manifold. Moreover, frozen stabilisation allows robust memory manifolds in small networks, and this is relevant to debates of implementing continuous attractors with a small number of neurons in light of recent experimental discoveries.

I. INTRODUCTION

Many biological systems are able to maintain a memory of relevant quantities in their dynamical states for durations much longer than the characteristic response time of the component parts. For instance, humans are able to hold information in working memory for durations much longer than the intrinsic timescales of neuronal responses. This fundamental and critical memory function is particularly relevant for neural systems, where the key challenges of implementing memory in networks of neurons have been extensively studied (c.f. [1] and references therein). If we consider the memory as being stored in the collective activity of the neurons, then the problem becomes one of implementing fixed-points in the network dynamics. Storing a discrete set of items can be achieved by having a discrete set of stable fixed-points in the dynamics; the Hopfield model [2] being a prominent example of such a memory.

Storing continuous variables in the dynamical state of a neural network is, fundamentally, a more difficult challenge. It requires a continuum of fixed-points forming a manifold, equipped with a structure that can preserve the metric information of the continuous variables. Such a continuous manifold attractor will be locally stable in directions normal to the manifold, and *marginally stable* along the manifold, so that the state can move smoothly along the manifold. Such a memory manifold can subserve critical functions such as evidence accumulation, path integration and more generally implementing flexible cognitive maps. Implementing such a manifold in a neural network has often required fine-tuned parameters and/or hand-crafted symmetries in the connectivity matrix [1, 3, 4]. Quoting [1], “[h]ow the brain might solve

this problem is an open theoretical and experimental question.”

Closely related to the problem of constructing memories is the problem of generating long timescales in the dynamics of neural networks ([5]; [6] pp. 329-250). This is motivated by the observation that the behaviours/outputs generated by these neural networks often display a wide spectrum of timescales much longer than the relevant timescales for individual neurons. In this case too, models for generating long timescales require fine-tuning of parameters.

The difficulty of constructing memory manifolds goes beyond neural networks and applies to dynamical models of biological systems more generally. For a dynamical system to function as a continuous memory, it needs to be poised between instability and stability – i.e. be marginally stable. This is typically achieved at bifurcation points, thus requiring parameters to be fine-tuned. Marginal stability without parameter fine-tuning necessarily requires the system to self-organise to a critical point, i.e. exhibit self-organised criticality – a highly non-trivial phenomenon. Apart from specific examples, more general principles to achieve this are lacking.

We present a principle that we refer to as *frozen stabilisation*, which allows a family of neural networks to self-organise to a state exhibiting memory manifolds and long timescales. The principle works by momentarily freezing/slowing the dynamics of a subpopulation of neurons, thereby creating a static background input which serves to stabilise the remaining population. These memory manifolds can function as general purpose integrators, and the emergence of the memory manifolds is robust to parameter choices and permits a wide range of connectivity matrices, including ones without any symmetries/structure.

* authors listed alphabetically;
correspondence: {tankut.can, kameshkk}@gmail.com

II. MEMORY MANIFOLDS IN A SIMPLE RECURRENT NETWORK

We first illustrate the frozen stabilisation principle by means of a specific neural network model, and then discuss the general principle which applies more broadly. Let us consider a recurrent neural network (RNN) described by the following dynamics:

$$\partial_t \mathbf{h} = \sigma(J^z \mathbf{h}) \odot \left[-\mathbf{h} + \frac{1}{2} J^h \phi(\mathbf{h}) \right] \quad (1)$$

Here, \mathbf{h} is a N -dimensional vector representing the internal states of the neurons, $J^{z,h}$ are $N \times N$ connectivity matrices, $\sigma(x) = [1 + e^{-\alpha x}]^{-1}$ is a sigmoidal non-linearity that acts element-wise and $\phi(x) = \tanh(gx)$ is the neuronal output nonlinearity with gain g . The entries of $J^{z,h}$ are sampled i.i.d from a centered Gaussian distribution with variance $1/N$. This is a variant of the ‘‘gated’’ RNN (gRNN) studied in [7]. We are interested in the limit of a binary sigmoid ($\alpha \rightarrow \infty$) and large N , where the network exhibits a self-organised marginally-stable phase over a wide range of parameters. To derive the conditions under which marginal stability is possible, we study the eigenvalues of the state-to-state Jacobian which describes the linearised dynamics. The system will be marginally stable when the spectral abscissa of the Jacobian is equal to zero. The Jacobian in this case is given by $\mathcal{D} = [\sigma](-\mathbb{1} + 1/2 J^h [\phi'])$, where $[\mathbf{x}]$ denotes a diagonal matrix with the vector \mathbf{x} on the diagonal. For large N , we can use non-Hermitian random matrix techniques along with mean-field theory, similar to [7], to calculate the spectral properties of the disorder-averaged Jacobian. The bounding spectral curve and the density near 0, will inform us about the stability and number of slow modes, respectively. It turns out that for $\alpha \rightarrow \infty$, the system will be marginally stable, with the spectral abscissa of \mathcal{D} poised at 0 and an extensive number of slow modes, provided the following condition is met:

$$\int \mathcal{D}x \left(\phi'(\sqrt{\Delta_h} x) \right)^2 < 8 \quad (2)$$

where $\mathcal{D}x$ is the standard Gaussian measure, and Δ_h is the mean-field (fixed-point) variance obtained from the self-consistency condition: $4\Delta_h = \int \mathcal{D}x \phi(\sqrt{\Delta_h} x)^2$. This corresponds to a range $2 < g \lesssim 6.2$ over which the network will self-organise to a marginally stable state with a large number of slow modes. Note that the matrices $J^{z,h}$, are completely unstructured.

In order to understand frozen stabilisation, it is instructive to study the dynamical mechanism which gives rise to the self-organised critical state in the gRNN. One might naively expect that in the limit $\alpha \rightarrow \infty$, the $\{\sigma\}$ terms go to zero and the h -variable becomes frozen, leading to fixed-points. However, with a little reflection it should be clear that at any given time the $\{[J^z h]_i\}$ will take both positive and negative values, and thus one should expect half the $\{\sigma_i\}$ to be zero and the other half to be 1 – i.e. half the $\{h_i\}$ are momentarily frozen and

the other half free to evolve. Moreover, we know from prior work that a ‘‘vanilla’’ RNN (vRNN) – where $\sigma_i = 1$ for all i in eq.1 – exhibits chaotic activity for $g > 2$ [7, 8]. So, in the gRNN, if half the $\{h_i\}$ are free to evolve what causes *all* the $\{h_i\}$ to be frozen – i.e. be at a fixed-point?

This is where the *stabilisation* in frozen stabilisation enters. We first take a detour to look at a simpler model: a vRNN with external random (fixed) biases. The dynamics for the vRNN with biases are given by equation below:

$$\dot{h}_i(t) = -h_i(t) + \frac{1}{2} \sum_{j=1}^{N/2} J_{ij}^v \phi_j(t) + \beta_i \quad (3)$$

where $J_{ij}^v \sim \mathcal{N}(0, 1/N)$ and $\beta_i \sim \mathcal{N}(0, \sigma_\beta^2)$; the superscript v is meant to denote the vanilla RNN. The factor of $1/2$ and the network size of $N/2$ (instead of N) are required to make the comparison to the gRNN meaningful. The coupling matrix J^v is of size $N/2 \times N/2$, but the elements are sampled from a centered Gaussian with variance $1/N$.

The effect of the random biases in the vRNN is to stabilise the dynamics – for a given g if σ_β exceeds a critical value, then the dynamics will flow to a stable fixed-point. Moreover, for a given set of biases $\{\beta_i\}$ there can only be *one* fixed-point. The critical value of σ_β can be obtained by analyzing the stability of the vRNN Jacobian which is given by:

$$\mathcal{D}_v = -\mathbb{1} + \frac{1}{2} J^v [\phi'(h)] \quad (4)$$

For large N , we can again use random matrix techniques to show that the leading edge of the spectrum will stable (< 0) provided: $\int \mathcal{D}x \left(\phi'(\sqrt{\Delta_h} x) \right)^2 < 8$. It is important to note that although this condition looks the same as eq. 2, the average here is taken with respect to variance obtained from the DMFT for eq. 3, by solving the following equation:

$$\Delta_h^v = \frac{1}{8} \Delta_\phi^v (\Delta_h^v) + \sigma_\beta^2 \quad (5)$$

This will give us a critical value for the variance of the biases $\sigma_\beta^*(g)$ (Fig. 1c, red line), above which the dynamics will flow to a (unique) stable fixed-point in the vRNN with biases.

In the case of the gRNN in the self-organised critical state, half the h -population is frozen and half is free to evolve; therefore, we can think of the frozen population as effectively providing random biases to the free-to-evolve population. We thus expect that the system will be at a fixed-point if the variance of the frozen population is larger than the critical variance of biases $\sigma_\beta^*(g)$ required to stabilise the evolving population, for the particular g . More specifically, we need to compare $\sigma_\beta^*(g)$ to the variance from the frozen population $\Delta_\phi^g/8$, where $\Delta_\phi^g =$

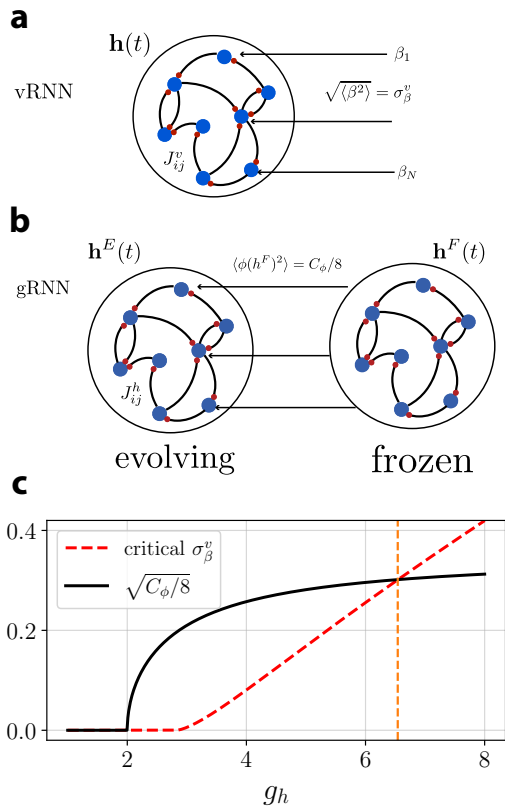


FIG. 1. *Illustrating frozen stabilisation in a RNN:* a) Schematic of the vanilla RNN (vRNN) with random biases (eq. 3). The dynamics will flow to a fixed-point if the variance of the biases is larger than a critical value $\sigma_\beta^{v*}(g)$. b) Schematic of the gated RNN (gRNN) where roughly half the population is frozen (\mathbf{h}^F) and roughly half is free to evolve (\mathbf{h}^E) at any given instant of time. The frozen half provides random biases to the evolving half as in (a). c) DMFT calculation of the variance of the frozen population in the gRNN (black line) and the critical variance required to stabilise the dynamics in the matched vRNN (dashed red line). For $2 < g \lesssim 6.2$ (till the orange line) the frozen population provides biases that can stabilise the evolving part.

$\langle \phi^2 \rangle$ is obtained by solving the fixed-point DMFT for the gated RNN:

$$\Delta_h^g = \frac{1}{4} \int \mathcal{D}x \phi(\sqrt{\Delta_h^g} x)^2 \quad (6)$$

Indeed, when we compare the critical variance of biases required to stabilise the matched vRNN $\sigma_\beta^{v*}(g)$, and the variance from the frozen-half of the population in the gRNN, the latter is larger for all g that satisfy eq. 2 (compare red and black lines in Fig. 1c). Thus, whenever g satisfies this condition and $\alpha = \infty$, the network self-organizes to a state where the *frozen* population acts as random biases that *stabilise* the free-to-evolve population, thus making the whole system marginally stable. It is important to emphasize that simply having half the σ_i frozen will not give rise to the self-organised state – i.e.

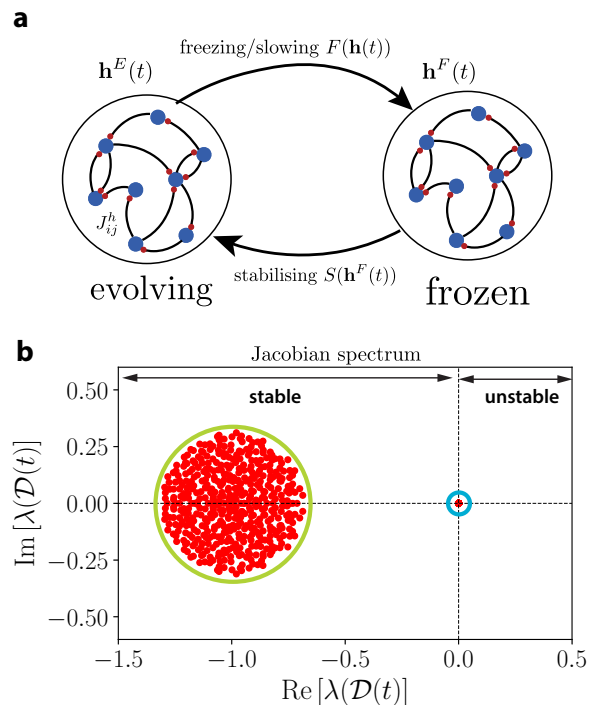


FIG. 2. *Frozen stabilisation through the lens of the Jacobian:* a) Schematic of a generic network exhibiting frozen stabilisation. A part of the system (\mathbf{h}^F) gets frozen instantaneously as a function of the full state, $F(\mathbf{h}(t))$. The frozen part in turn stabilises the evolving part, (\mathbf{h}^E), by means of the interactions $S(\mathbf{h}^F(t))$. b) The Jacobian spectrum of a generic system exhibiting frozen stabilisation. Any freezing mechanism gives rise to an accumulation of eigenvalues at zero (blue circle), and if the frozen part can sufficiently stabilise the evolving part, then the remaining eigenvalues will be in left half-plane (green circle).

there is no marginal stability for $g > 6.2$ (orange line in Fig.1c). As will be shown below the self-organised state is characterised by a continuum of connected fixed-points – i.e. a memory manifold.

III. FROZEN STABILISATION AS A GENERAL PRINCIPLE TO PRODUCE MEMORY MANIFOLDS

The mechanism discussed in the context of the gRNN, where one part of the system that is dynamically/momentarily slowed, stabilises the freely evolving part, forms the core of the principle of frozen stabilisation for achieving the memory manifolds. Although, we illustrated the principle with a specific model, we will see that it is more general and does not depend on the specific parameter and connectivity choices of the gRNN. To see this, it is instructive to look at the marginally-stable state through the lens of the state-to-state Jacobian. Fig.

2a, shows a schematic of a system displaying frozen stabilisation and the accompanying Jacobian spectrum. The main requirement for the principle is that one part of the system (\mathbf{h}^F) gets instantaneously slowed/frozen depending on the state of the whole system (depicted by $F(\mathbf{h}(t))$ in Fig. 2a). The freezing function F we consider in the case of the gRNN are the switch-like binary gates with tuneable biases, $F(\mathbf{h}) = \sigma(J^z \mathbf{h})$ but in principle, this could be more general. The frozen population in turn stabilises the evolving population by means of the interactions $S(\mathbf{h}^F(t))$. In the case of the gRNN above, the stabilisation function $S(\mathbf{h}^F) \equiv +J^{h,F} \phi(\mathbf{h}^F)/2$ corresponds to additive interactions – i.e. biases; however, this too can, in principle, be more general. Fig. 2b shows the generic Jacobian spectrum for a system displaying frozen stabilisation: *any* freezing mechanism will lead to an accumulation of slow modes near zero (blue circle in Fig. 2b) and if the frozen population can stabilise the evolving population then all the remaining Jacobian eigenvalues will have real parts less than 0 (green circle in Fig. 2b). As long as the Jacobian spectrum has this general form, we will have a system that generates a memory manifold. Since the only requirement for stable eigenvalues is that they have real parts less than 0, the principle is not slave to precise connectivity matrices with special symmetries or fine-tuned parameters. Indeed, the principle will work even with diagonal J^z , correlations between the elements of J^h and other activation functions ϕ , such as the rectified-linear function (ReLU). We will study this robustness in more detail below.

A. A self-stabilised RNN using frozen stabilisation

Armed with the key features of frozen stabilisation, we can now embark on constructing a variety of RNNs which produce a memory manifold. Here we give one example of a network that can generate a memory manifold even with ~ 20 neurons: the self-stabilised RNN (ssRNN). In the case of the ssRNN, we make use of the fact that larger bias variances of the frozen population will lead to more robust stabilisation. We incorporate a dynamical variable that modulates the variance of the frozen population, thereby ensuring robust frozen stabilisation over a much wider range of parameters compared to the gRNN. The dynamics of the ssRNN are given by the following equations:

$$\begin{aligned} \partial_t \mathbf{h} &= \boldsymbol{\sigma}_1 \odot [-\mathbf{h} + J^h(\phi \odot \boldsymbol{\sigma}_2)], \\ \boldsymbol{\sigma}_1 &= \Theta(J^z \phi + \beta_1), \\ \boldsymbol{\sigma}_2 &= \gamma [\mu_\sigma(t)(1 - \boldsymbol{\sigma}_1) + G(1 - \mu_\sigma(t))\boldsymbol{\sigma}_1] \end{aligned} \quad (7)$$

where $\Theta(\cdot)$ denotes the Heaviside function, $\mu_\sigma(t) = \langle \boldsymbol{\sigma}_1(t) \rangle$ is the mean (instantaneous) fraction of freely evolving neurons and G is a gain control parameter chosen to be ≤ 1 . The bias β_1 controls μ_σ and thus the dimensionality of the memory manifold.

The self-stabilising nature of the network is evident

from $\boldsymbol{\sigma}_2$: when the size of the evolving population is larger than the frozen population then $\boldsymbol{\sigma}_2$ dynamically boosts the output of the frozen population and suppresses the outputs of the evolving part thereby ensuring that the frozen part can stabilise the evolving part. This ensures that the network exhibits a memory manifold over a very wide range of g .

Another way to see the stabilisation in the ssRNN is to focus on the spectrum of the state-to-state Jacobian and examine what values of g destabilise the system. In the gRNN, larger values of g destabilise the network and lead to chaotic activity. Specifically, for a gRNN of size N where the weights have variance $1/N$, the g that destabilises the system is found by solving $\langle (\phi')^2 \rangle = 8$. A similar condition for the instability of the Jacobian (see Appendix A for details) in the ssRNN leads to the realisation that the self-stabilisation mechanism effectively rescales the neuronal gain, yielding a lower effective g given by

$$g_{eff}^2 = G^2 g^2 \mu_\sigma (1 - \mu_\sigma)^2 \quad (8)$$

The self-stabilisation also allows the ssRNN to implement the memory manifold with just a few neurons. Indeed, in Fig. 7 we see that a ssRNN with $N = 50$ has a Jacobian that shows robust frozen stabilisation.

We would like emphasise that the ssRNN is just one example of a family of RNNs that can exploit frozen stabilisation to generate a memory manifold. The key requirement is that the frozen population is able to stabilise the freely evolving population thus pushing the non-zero eigenvalues of the Jacobian to the left of the imaginary line, as in Fig. 2b. As long as the Jacobian has this form, the system will generate a memory manifold. Indeed, this principle can be implemented even in a network with $N = 3$, which allows us to visualise the manifold as we see below. We now proceed to study the properties of the memory manifold produced by frozen stabilisation.

IV. PROPERTIES OF THE MEMORY MANIFOLD

A. Robustness of Frozen Stabilisation

As we indicated above, frozen stabilisation and the emergence of the associated memory manifold are not slave to the details of the precise connectivity matrices, and do not require fine-tuned gain parameters. Here, we consider the effects of perturbations to parameters, and connectivity matrices that might be more biologically relevant. In networks of real neurons, a salient deviation for the completely unstructured connectivity is the over-representation of bidirectional connections suggesting a partially symmetric structure (e.g. [9, 10]). We can study the effects of such structure on the manifold by considering matrices J^h that can vary between fully symmetric to fully anti-symmetric. Specifically, we consider J^h from the elliptic ensemble ([11]) where $\langle (J_{ij}^h)^2 \rangle = N^{-1}$

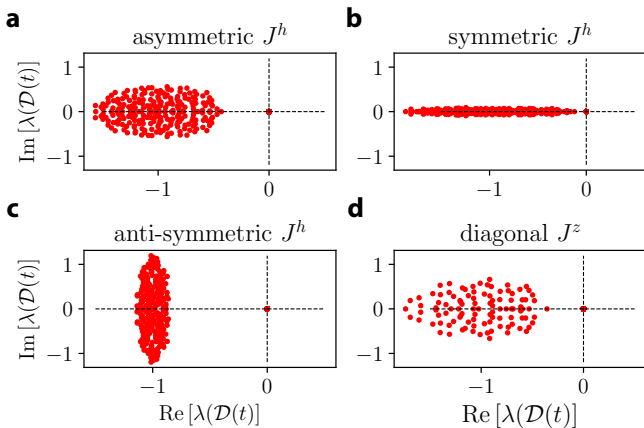


FIG. 3. *The emergence of the memory manifold is robust to choices of the connectivity matrices $J^{h,z}$* (a-c) Jacobian spectrum of a ssRNN with J^h from an elliptic ensemble to model asymmetric (a, $\eta = 0$), symmetric (b, $\eta = 0.8$) or anti-symmetric (c, $\eta = -0.8$) interactions. d) Same ssRNN as (a), but with a diagonal J^z with random ± 1 on the diagonal. Parameters of the ssRNN: $N = 500$, $g = 2.0$, $G = 1.0$.

and $\langle J_{ij}^h J_{ji}^h \rangle = \eta N^{-1}$, with $\eta \in [-1, 1]$. The symmetric, asymmetric and anti-symmetric cases correspond to η being 1, 0 and -1 , respectively. In Fig.3 a-c, we see representative examples with the ssRNN wherein, other parameters being the same, introducing strong symmetry or anti-symmetry in J^h does not affect the emergence of the memory manifold since the non-zero eigenvalues of the Jacobian are still stable [12].

Another salient difference in the connectivity is the choice of J^z which governs how the freezing variable σ_1 depends on \mathbf{h} . In particular, when J^z is diagonal, this would imply that the freezing variable is local – i.e. $\sigma_{1,i}$ only depends on h_i . This choice too does not hamper the formation of the memory manifold, as is shown in an illustrative example in Fig. 3d.

Thus far, we looked at choices for the connectivity matrices, let us now briefly consider whether the memory manifold will fall apart if the connection matrices or the gain parameters are perturbed. For random connectivity matrices $J^{z,h}$ and large N , if each J_{ij}^h is independently perturbed by an amount $N^{-1}\delta \cdot \xi_{ij}$, then the effect of this perturbation is similar to increasing g , and as long as the spectral edge of the non-zero eigenvalues of the Jacobian does not cross zero, the memory manifold will still exist; this will be the case when g is not close to the boundaries of its permissible range. In contrast, low-rank perturbations of the form $J^h \rightarrow J^h + uu^T$ can potentially push some of the zero eigenvalues to positive values, thus destabilising the slow manifold; the particular detrimental perturbations will depend on the model details.

B. True continuum of fixed-points

A salient feature of the memory manifold generated by frozen stabilisation is that it is a continuum of marginally stable fixed-points. This is in contrast to previous models to generate continuous attractors [1, 13, 14], where a continuous manifold is approximated by a discrete set of $O(N)$ fixed-points, where N is the system size (no. of neurons). The distinction matters for the resolution with which the continuous variable can be stored or “quantised”; specifically, a manifold of dimension D that is approximated with N fixed-points will have a resolution that scales as $N^{-1/D}$, and this can deteriorate rapidly with D , even for small D .

To see that a network exhibiting frozen stabilisation does indeed give us a continuum of fixed-points and not a discrete set, let us consider the gRNN from before – the argument will work with any other network exhibiting frozen stabilisation. It is sufficient to study how the network responds to infinitesimal perturbations away from a particular fixed-point. In the gRNN, denoting the frozen population by h^F , and the active population by h^E , we find that for a neuron in the evolving population, at a fixed point the following equation must hold,

$$0 = -h_i^E + \frac{1}{2} \sum_{i \in E} J_{ij}^h \phi(h_i^E) + \frac{1}{2} \sum_{\mu \in F} J_{i\mu}^h \phi(h_\mu^F) \quad (9)$$

If we now apply an infinitesimal perturbation $h^F \rightarrow h^F + \delta h^F$, then as long as the evolving population can still accommodate a fixed-point by adjusting infinitesimally as $h^E \rightarrow h^E + \delta h^E$, the manifold will be continuous. This is possible as long as the following equation has a solution:

$$\left(\mathbb{I} - \frac{1}{2} \tilde{J}^E \phi'(h^E) \right) \delta h^E = \frac{1}{2} \tilde{J}^F \phi'(h^F) \delta h^F. \quad (10)$$

There is a solution to eq. 10 if the matrix in parentheses on the LHS is invertible. Since the leading edge of this matrix is at $1 - \frac{1}{8} \langle \phi'^2 \rangle$ – for large N – invertibility is guaranteed when eq. 2 is true, i.e., in the marginally stable region. Thus, so long as the network exhibits frozen stabilisation, there will exist a continuous manifold of fixed-points. The same argument, can be easily extended to link the stability of the Jacobian to the continuity of the manifold for other networks, like the ssRNN in Fig. 7, exhibiting frozen stabilisation. The fact that frozen stabilisation allows networks with a small number of neurons to exhibit continuous manifolds is potentially relevant to questions about achieving continuous attractors with a few neurons in the nervous systems of insects [15, 16].

C. Geometry of the memory manifold

Having demonstrated the continuity of the memory manifold, we now study some of its geometric proper-

ties. From the arguments about the continuity of the manifold above, it should be evident that the frozen population (\mathbf{h}^F) forms a natural set of coordinates for the memory manifold. This can also be understood by considering the structure of the left- and right-eigenvectors of the Jacobian. For the sake of illustration, let us consider the gRNN. Then the left-eigenvectors L_μ for the zero eigenvalues satisfy:

$$L_\mu^T \mathcal{D} = 0 \quad \text{where } \mathcal{D} = [\boldsymbol{\sigma}](-\mathbb{1} + 1/2 J^h[\boldsymbol{\phi}']). \quad (11)$$

For every frozen neuron with $\sigma_\mu = 0$, there exists a left-eigenvector of the form $L_\mu^T = (0, \dots, 1, \dots, 0)$, with a single zero at location μ , that satisfies eq. 11. The dimensionality of the slow manifold is the number of linearly independent zero modes, which is precisely the size of the frozen population. We also note that biorthogonality implies that the right-eigenvectors R_μ corresponding to the zero eigenvalues are supported on exactly one frozen dimension, and the rest of the support is spread over the evolving population.

In the gRNN, the size of the frozen population is $N/2$, and thus the manifold is high-dimensional. In the ssRNN we can have a lower-dimensional manifold, not only because the network can support manifolds for smaller N , but also due to the ability to achieve stable manifolds with a smaller fraction of frozen neurons by tuning β_1 in eq. 7. Thus, the ssRNN offers a way to tune the dimensionality for a fixed N .

We now proceed to calculate the metric tensor $g_{\mu\nu}$ for the memory manifold, which informs us about the local geometry of the manifold. The manifold is embedded in R^N , parametrised by the coordinates \mathbf{h}^F , and the metric prescribes infinitesimal distances as $ds^2 = g_{\mu\nu} dh^{F,\mu} dh^{F,\nu} = |\mathbf{d}\mathbf{h}^F|^2 + |\mathbf{d}\mathbf{h}^E|^2$, where summation over repeated indices is implied, and $\mathbf{d}\mathbf{h}_i^E = (dh_i^E/dh_\mu^F) dh_\mu^F$. This gives us

$$g_{\mu\nu} = \delta_{\mu\nu} + \sum_{i \in E} \frac{dh_i^E}{dh_\mu^F} \frac{dh_i^E}{dh_\nu^F} \quad (12)$$

Before we calculate eq. 12 for a specific model, we make a general note: for the models we have so far discussed, the metric takes the form

$$g_{\mu\nu} = \delta_{\mu\nu} + \phi'(h_\mu^F) \phi'(h_\nu^F) \Gamma_{\mu\nu} \quad (13)$$

where Γ is a matrix that will depend on the model. We immediately note the explicit dependence of the metric on the non-linearity $\phi(\cdot)$. In particular, if $\phi(\cdot)$ is a piecewise linear function, such as $\phi(x) = \max(0, x)$, then the metric is *locally flat*, i.e. $g_{\mu\nu} \propto \delta_{\mu\nu}$.

For the gRNN, we can appeal to random-matrix techniques to give an explicit form for the average metric (c.f. Appendix B for details), [17]:

$$\mathbb{E}[g_{\mu\nu}] = \delta_{\mu\nu} \left[1 + \frac{(\phi'(h_\mu^F))^2}{8 - \langle (\phi')^2 \rangle} \right] + O(N^{-1}) \quad (14)$$

1. Global geometry of the manifold

Having considered the local geometry above, we now make a few remarks on the global geometry of the manifold. In general, the global geometry of the manifold (embedded in R^N) can be quite complicated and even the dimensionality can change from one part of the phase space to the other. In Fig. 4, we see an example of the (2-D) manifold embedded in R^3 , for a gRNN with $N = 3$. The manifold was generated by sampling initial conditions from a grid in R^3 , and running the forward dynamics till convergence to a fixed-point (see Appendix B 1 for details of the numerics). We see that the global structure consists of two ‘‘sheets’’ (red & green in Fig. 4) that are connected – each sheet corresponds to a different subset of (2) frozen units. Note that the sheets themselves are continuous, and the discreteness is an artefact of the sampling. This picture of the global structure consisting of continuous sheets that are stitched together also holds in higher dimensions, and each sheet corresponds to a particular subset of units being frozen. Which particular subset of units contribute to any particular sheet is controlled by the J^z matrix, and the J^h matrix controls the stability.

V. A GENERAL PURPOSE INTEGRATOR

One of the crucial functions a memory manifold can implement is that of a general purpose integrator: external input along the manifold directions will move the state on the manifold, and once the input ceases, the final state will store the integrated value of the input; however, traces of inputs that are not aligned to the manifold will decay away rapidly. Integrator function of this type forms the basis of several biologically important computations such as evidence accumulation [18, 19], path integration [14], and more generally implementing cognitive maps [20, 21]. It is well known that implementing an integrator in biologically realistic models requires fine-tuning and special symmetries [1, 3, 6]. Frozen stabilisation might offer a possible way for biological systems to implement the integrator function over a wide range of parameters and interaction patterns. In Fig. 5 we see an example of this integrator function: inputs lasting a short duration (5 time units) are applied along different directions of the memory manifold produced by a ssRNN, at times indicated by the vertical dashed lines. The projection of the network state $\mathbf{h}(t)$ on the input directions shows that the state integrates the input and maintains it in memory for a long time; moreover, the traces of inputs along the different directions do not interfere with each other. Another salient feature of frozen stabilisation is that it allows a truly continuous integrator to be robustly implemented in systems with low dimensionality (e.g. ssRNN with $N \sim 20$). This is in contrast with the classical models for continuous attractors in neural systems (e.g. [13, 14]) where the number of fixed-points,

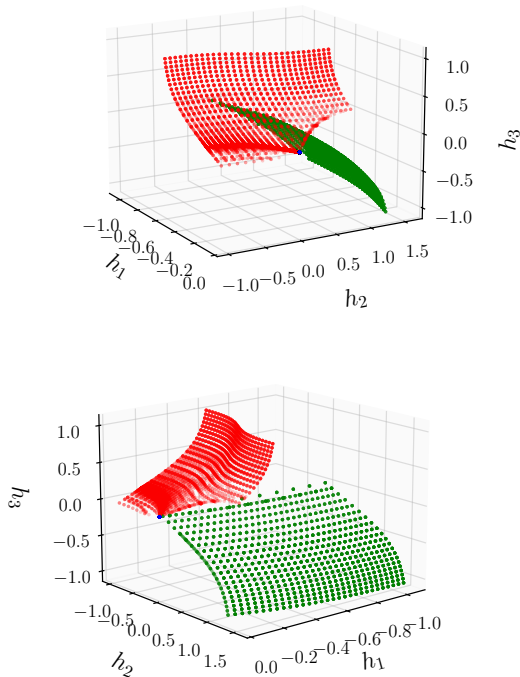


FIG. 4. *Global geometry of the memory manifold*

Two views of an example 2-D manifold generated by a gRNN with 3 units. The global structure consists of two “sheets” (red & green) that are connected. Each sheet consists of a distinct subset of 2 frozen units. The manifold was generated by sampling a grid of initial conditions in $[-1, 1]^3$ and running the dynamics till a fixed-point was reached (further details about numerics in Appendix B 1).

and thus the integrator resolution, scale with the system size, N . Recent experimental work in the nervous system of insects has provided evidence for integrators with continuous attractor dynamics for representing angular orientation with a small no. (~ 20) of neurons [16]. If we use the classical models in their original form, it raises the problematic question of the resolution of the angular representation. Memory manifolds generated by frozen stabilisation, thus, might be relevant to debates about achieving continuous attractors with a small number of neurons.

VI. LONG TIMESCALES WITHOUT FINE-TUNING

Now we consider a problem that is closely related to the problem of memory: generating long timescales. How can a system generate timescales in its collective dynamics, which are much longer than the intrinsic timescale of its units? Typical examples of achieving this require a system to be close to a bifurcation point in the param-

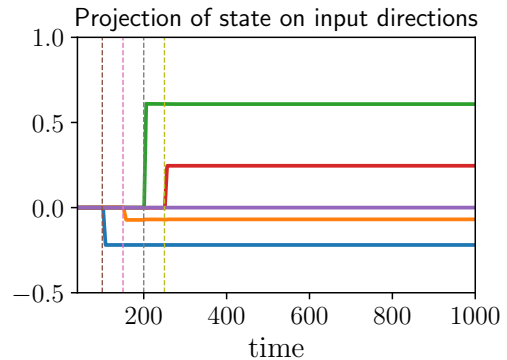


FIG. 5. *Memory manifold can be used as an integrator:* Input pulses lasting 5 time units, with random amplitudes, are applied along randomly selected manifold directions starting at the times indicated by the vertical dashed lines. The (excess) projection of the state on the input directions shows that the input trace is integrated and retained in the network state $\mathbf{h}(t)$ for a long time. Moreover, the inputs along different directions do not interfere with each other. The network used is a ssRNN with $g = 1.0$, $N = 100$, $G = 1.0$.

eter space – i.e. fine-tuning of parameters is needed. In general, achieving long timescales without fine-tuning is challenging [3, 5, 6].

From the discussion of frozen stabilisation above, we know that for a wide range of parameters (e.g. $2 < g \lesssim 6.2$ for the gRNN), and binary σ the dynamics will flow to marginally-stable fixed-points – i.e. have infinitely long timescales. Moreover, these timescales are generated, not by fine-tuning parameters, but by the network self-organising to a critical state. Indeed, requiring the system to be marginally stable over a range of parameters necessitates self-organising to a critical point.

Here, we would like to extend the discussion of self-organised generation of long timescales to the case when σ is sensitive but not binary. We can parametrise the sensitivity with a gain α such that $\sigma(x) = [1 + \exp(-\alpha x)]^{-1}$; $\alpha \rightarrow \infty$ would give the binary case. For concreteness, let us consider the case of the gRNN with large-but-finite α . In Fig. 6a, we see that for large α the dynamics for the network still exhibit timescales that are many orders of magnitude larger than the intrinsic timescale of a neuron (τ_h). Like the strictly marginally-stable state these long timescales are a self-organized phenomenon and not simply the result of having a sensitive σ ; indeed for g outside the range supporting marginal stability, the exact same network exhibits overall fast chaotic dynamics (Fig. 6a, inset), with only intermittent short-lived freezing of activity.

It is instructive to study features of this self-organised behaviour using the “velocities” $|\partial_t h_i(t)|$. In Fig. 6b,c we see that the characteristic feature of this dynamical state is that after short transients the velocities $\partial_t h_i(t)$ are quickly suppressed to very low values for *every* neuron (see red lines in Fig. 6b,c), even though the population

averaged values of other quantities such as $\langle h_i(t) \rangle$ may be biased away from zero (the expected value). [22] We also see that roughly half the σ_i are open and roughly half are closed – compare the mean and standard-deviation of $\{\sigma_i(t)\}$ (orange lines in 6b,c). This means that half the h -population is free to evolve. Thus, the collective dynamics gives us access to long timescales over a wide range of values for g and α . As a final point, how long are the long timescales in this regime of large-but-finite α ? Simple diffusion arguments suggest that these timescales should be closely related to the timescale for the σ_i switching which will scale as $\tau_{switch} \sim \alpha^2 \langle \phi(h)^2 \rangle$.

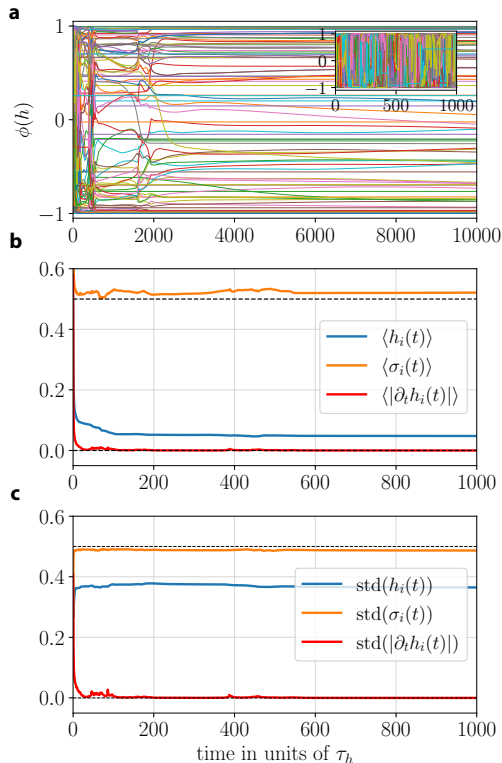


FIG. 6. *Emergent long timescales*: a) Sample traces of a gRNN exhibiting long timescales in the collective dynamics : $N = 1000, \alpha = 50, g = 4.0$; (inset) same network but with $g = 8.0$ shows fast, chaotic dynamics. b,c) Mean(b) and standard deviation(c) of population averaged quantities, showing that the velocity ($|\partial_t h_i(t)|$) for all neurons are rapidly suppressed after short transients. Note that half of the σ_i are open are open at any given instant.

VII. DISCUSSION

In this work we address two long-standing challenges that arise in the context of neural networks, and dynamical models of biological systems more broadly: i) how to implement a memory for continuously varying quantities without using special symmetries or fine-tuning parameters; and ii) how to generate long timescales in the collec-

tive dynamics without fine-tuning parameters. The ability to implement memory and generate long timescales underlies several functions critical for survival such as evidence accumulation from a noisy signal [18, 19], path integration based on velocity cues [14], implementing cognitive maps [20, 21], just to name a few. Implementing memory/long timescales requires the system to be poised at the edge of stability-instability, and prior approaches to this problem have typically relied on systems close to a bifurcation point, thus requiring tuning parameters to a special value. Marginal stability without symmetries or parameter fine-tuning requires the system to dynamically self-organize into a critical state. This is a highly non-trivial phenomenon, and apart from specific models, more general principles are hard to come by.

Here we present a principle that we refer to as *frozen stabilisation*, which allows a family of models to self-organise to a critical state to generate a continuous memory manifold and long timescales. The principle is robustly implemented over a range of parameter and doesn't require any symmetries in the interactions of the system. Moreover, systems exhibiting frozen stabilisation yield a true continuum of fixed-points, unlike prior models where the manifold is approximated by a discrete set of fixed points that scale with the system size. This is relevant to debates about achieving continuous attractors in neural systems with a small number of neurons, which have become important in light of the experimental results on the fly navigation system [16]. To our knowledge, frozen stabilisation is the first example of a principle that allows robust implementation of continuous attractors in small systems.

We discussed the principle of frozen stabilisation using examples of specific neural network models, and a salient feature of these models was the binary σ variable that momentarily slowed down a part of the system depending on the instantaneous system state. One natural question that arises is whether frozen stabilisation can be implemented without the binary σ ? If we consider a more general class of dynamical systems specified by $\partial_t \mathbf{h}(t) = F[G(\mathbf{h})]$, where F is a function acts element-wise, and has some regions of its domain where $F(x) = 0$ (e.g. $F = \max(0, x)$) then units for which $G(h_i)$ fall in those regions will be momentarily frozen and one can in principle achieve frozen stabilisation depending on the form of $G(\cdot)$. More generally, the discussion of frozen stabilisation through the lens of the Jacobian spectrum suggests a larger family of dynamical systems could yield the form of the spectrum required to exhibit frozen stabilisation. We leave characterising fully, the classes of systems in which this principle can be implemented for future work. Another aspect that needs further investigation is the geometric properties of the memory manifold. The global geometry of the manifold is strongly shaped by the interactions in J^z , and in the current examples we have discussed random/unstructured matrices and the manifolds that result. One could potentially imagine learning rules that might shape J^z to yield certain target geome-

tries.

In summary, we have presented a principle that allows for robust implementation of continuous memories and long timescales in neural networks, without fine-tuning parameters or using special symmetries. Such memory networks could be useful to model biological implementations of integrators or cognitive maps. These networks could also serve as “memory reservoir” modules for use larger machine learning architectures requiring information processing over long timescales.

ACKNOWLEDGMENTS

KK is supported by a C.V. Starr Fellowship and a CPBF Fellowship (through NSF PHY-1734030).

Appendix A: Details of the ssRNN

In this section, we outline the calculation for the Jacobian spectrum of the ssRNN, and the effective gain g_{eff} . The dynamics of the ssRNN are given by eq. 7, however, we consider here a slightly more general formulation allowing for non-binary sigmoids. Consider the ssRNN with the following dynamics

$$\dot{h}_i = \sigma_1(z_i) (-h_i + J_{ij}^h \phi(h_j) \sigma_2(z_j)) \quad (\text{A1})$$

$$\sigma_2(z_j) = \mu_f (1 - \sigma_1(z_j)) + \mu_a \sigma_1(z_j) \quad (\text{A2})$$

$$\tau \dot{z}_i = -z_i + J_{ij}^z \phi(h_j) \quad (\text{A3})$$

where $\sigma_{1,2}(x) = [1 + \exp(-(\alpha_{1,2}(x + \beta_{1,2})))]^{-1}$. We get back eq.7 in the limit $\alpha_{1,2} \rightarrow \infty$ and $\tau, \beta_2 \rightarrow 0$. The Jacobian at a fixed-point is then given by

$$\mathcal{D} = \begin{pmatrix} [\sigma_1](-\mathbb{1} + J^h[\phi' \circ \sigma_2]) & [\sigma_1]J^h[\phi \circ \sigma_2'] \\ J^z[\phi']/\tau & -\mathbb{1}/\tau \end{pmatrix} \quad (\text{A4})$$

The Jacobian depends on the random matrices $J^{z,h}$, but for large N , we can leverage tools from non-Hermitian random matrix theory, to calculate the bounding spectral curve of the disorder-averaged Jacobian. The details can be found in [7, 23]. Here we only provide the final expression. The bounding spectral curve is given by all points $\lambda \in \mathbb{C}$ such that

$$1 = \left\langle \frac{[\phi'(h)\sigma_2(z)\sigma_1(z)]^2}{|\lambda + \sigma_1(z)|^2} \right\rangle + \frac{\langle [\phi(h)\sigma_2'(z)]^2 \rangle}{|\tau\lambda + 1|^2} \left\langle \frac{[\phi'(h)\sigma_1(z)]^2}{|\lambda + \sigma_1(z)|^2} \right\rangle \quad (\text{A5})$$

The angular brackets denote averages w.r.t independent Gaussian variables h, z whose variances satisfy the fixed-point mean-field equations. Having derived the

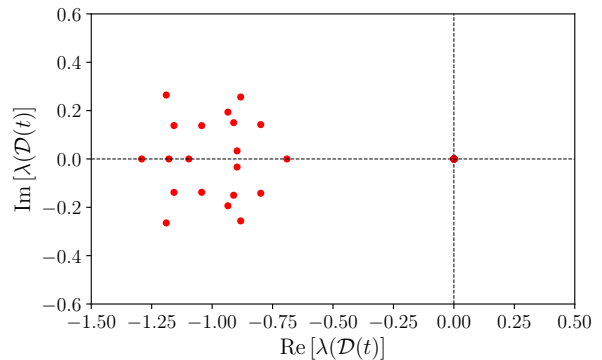


FIG. 7. *ssRNN with 50 neurons*

more general spectral curve, we now consider the limit $\tau \rightarrow 0$ and $\alpha_{1,2} \rightarrow \infty$ and $\mu_a = G(1 - \mu_{\sigma_1})$. In this limit we get

$$|\lambda + 1|^2 = G^2 \langle \phi'^2 \rangle \mu_{\sigma} (1 - \mu_{\sigma})^2 \quad (\text{A6})$$

where the variance of the Gaussian field h , Δ_h is determined from the condition

$$\Delta_h = G^2 \mu_{\sigma_1} (1 - \mu_{\sigma_1})^2 \int \mathcal{D}x \phi(\sqrt{\Delta_h}x)^2 \quad (\text{A7})$$

$$\mu_{\sigma_1} = \int \mathcal{D}x \Theta(x + \beta_1) \quad (\text{A8})$$

From eqs. A6, A7, we get the equation for the effective g . We note that even though we have used the MFT for large random RNNs in this section, an ssRNN with 50 neurons also shows robust frozen stabilisation (see Fig. 7)

Appendix B: Details of the manifold geometry

In this section, we provide the details of calculating the metric tensor $g_{\mu\nu}$ and the local curvature for the gRNN. As before, we split the population into a frozen part \mathbf{h}^F and an evolving part \mathbf{h}^E . At a fixed-point, we have

$$0 = -h_i^E + \frac{1}{2} \sum_{j \in E} J_{ij}^h \phi(h_j^E) + \frac{1}{2} \sum_{\mu \in F} J_{i\mu}^h \phi(h_{\mu}^F) \quad (\text{B1})$$

and thus, we can express dh_i^E/dh_{μ}^F as

$$\frac{dh_i^E}{dh_{\mu}^F} = \frac{1}{2} \sum_{j \in E} J_{ij}^h \phi'(h_j^E) \frac{dh_j^E}{dh_{\mu}^F} + \frac{1}{2} J_{i\mu}^h \phi'(h_{\mu}^F) \quad (\text{B2})$$

We can express all this compactly in matrix form. Denoting by $\tilde{J}^E \in \mathbb{R}^{N_E \times N_E}$, the connectivity matrix between

the evolving population, and by $\tilde{J}^F \in R^{N_E \times N_F}$ the connectivity matrix between the frozen and excitatory populations, we get

$$\underbrace{\left(\mathbb{1} - \frac{1}{2} \tilde{J}^E [\phi'(\mathbf{h}^E)] \right)}_{\mathcal{D}_E} \frac{d\mathbf{h}^E}{d\mathbf{h}^F} = \frac{1}{2} \tilde{J}^F [\phi'(\mathbf{h}^F)] \quad (\text{B3})$$

From eq. 12, we get

$$g_{\mu\nu} = \delta_{\mu\nu} + \frac{1}{4} \left[(\tilde{J}^F [\phi'(\mathbf{h}^F)])^T (D_E D_E^T)^{-1} (\tilde{J}^F [\phi'(\mathbf{h}^F)]) \right]_{\mu\nu} \quad (\text{B4})$$

For large N , we can calculate the average metric $\mathbb{E}[g_{\mu\nu}]$ by averaging over the connectivity matrix. To proceed, we denote the fraction of frozen neurons as $f \equiv N_F/N$, and note that for a general matrix A to leading order in N ,

$$\langle (\tilde{J}^F)^T A \tilde{J}^F \rangle = (1-f) \frac{1}{N_E} \text{Tr}[A] \equiv (1-f) \text{tr}[A] \quad (\text{B5})$$

Thus, we can simplify eq. B4 by first averaging over \tilde{J}^F :

$$g_{\mu\nu} = \delta_{\mu\nu} \left[1 + (1-f) (\phi'(h_\mu^F))^2 \text{tr}[(D_E D_E^T)^{-1}] \right] \quad (\text{B6})$$

Interestingly, after averaging over \tilde{J}^F , the metric is diagonal. Now, we are left to evaluate the average of the trace term, which involves \tilde{J}^E . From, eq. using the series expansion for \mathcal{D}_E^{-1} , we get

$$(D_E D_E^T)^{-1} = \sum_{m,n} \left(\frac{1}{2} [\phi'] (\tilde{J}^E)^T \right)^m \left(\frac{1}{2} \tilde{J}^E [\phi'] \right)^n \quad (\text{B7})$$

when we average over \tilde{J}^E , only the ‘‘non-crossing’’ diagrams contribute to leading order in N . These diagrams come from terms for which $m = n$. We thus get

$$\text{tr}[(D_E D_E^T)^{-1}] = (1 - (1-f) \langle (\phi')^2 \rangle)^{-1} \quad (\text{B8})$$

Putting it all together, we can express the average metric as

$$\mathbb{E}[g_{\mu\nu}] = \delta_{\mu\nu} \left[1 + \frac{(1-f) (\phi'(h_\mu^F))^2}{4 - (1-f) \langle (\phi')^2 \rangle} \right] \quad (\text{B9})$$

In the case, when the populations are symmetric $f = 1/2$, and this simplifies to

$$\mathbb{E}[g_{\mu\nu}] = \delta_{\mu\nu} \left[1 + \frac{(\phi'(h_\mu^F))^2}{8 - \langle (\phi')^2 \rangle} \right] \quad (\text{B10})$$

1. Details of the numerics for global geometry

Here we provide the details for generating Fig. 4. We use a gRNN with the following parameters: $N = 3, g = 2.0$ and the following connectivity matrices:

$$J^h = \begin{pmatrix} -0.14 & 0.13 & -0.62 \\ -0.45 & -0.19 & -1.50 \\ 0.27 & -0.28 & -1.16 \end{pmatrix} \quad (\text{B11})$$

$$J^z = \begin{pmatrix} 0.57 & -0.26 & 0.95 \\ 0.02 & 0.27 & -0.46 \\ 1.0 & -0.04 & -0.04 \end{pmatrix} \quad (\text{B12})$$

The initial conditions are sampled from a grid in the cube $[-1, 1]^3$, and the dynamics are run till a fixed-point is reached. The final state is plotted, with a color indicating which subset of the 3 neurons are part of the frozen population.

-
- [1] R. Chaudhuri and I. Fiete, *Nature neuroscience* **19**, 394 (2016).
- [2] J. J. Hopfield, *Proceedings of the national academy of sciences* **79**, 2554 (1982).
- [3] H. S. Seung, *Proceedings of the National Academy of Sciences* **93**, 13339 (1996).
- [4] H. S. Seung, *Neural Networks* **11**, 1253 (1998).
- [5] X. Chen and W. Bialek, *arXiv preprint arXiv:2008.11674* (2020).
- [6] W. Bialek, *Biophysics: searching for principles* (Princeton University Press, 2012).
- [7] K. Krishnamurthy, T. Can, and D. J. Schwab, *arXiv preprint arXiv:2007.14823* (2020).
- [8] H. Sompolinsky, A. Crisanti, and H.-J. Sommers, *Physical review letters* **61**, 259 (1988).
- [9] H. Markram, J. Lübke, M. Frotscher, A. Roth, and B. Sakmann, *The Journal of physiology* **500**, 409 (1997).
- [10] Y. Wang, H. Markram, P. H. Goodman, T. K. Berger, J. Ma, and P. S. Goldman-Rakic, *Nature neuroscience* **9**, 534 (2006).
- [11] H. J. Sommers, A. Crisanti, H. Sompolinsky, and Y. Stein, *Physical review letters* **60**, 1895 (1988).
- [12] As an aside, the non-zero bulk of the Jacobian spectrum strongly resembles the spectrum of J^h from the elliptic ensemble, this is because the relevant block of the Jacobian has the form $\tilde{J}P$ where P is a positive diagonal matrix and \tilde{J} is from the elliptic ensemble.
- [13] R. Ben-Yishai, R. L. Bar-Or, and H. Sompolinsky, *Proceedings of the National Academy of Sciences* **92**, 3844 (1995).
- [14] Y. Burak and I. R. Fiete, *PLoS computational biology* **5**, e1000291 (2009).
- [15] D. B. Turner-Evans, K. T. Jensen, S. Ali, T. Paterson, A. Sheridan, R. P. Ray, T. Wolff, J. S. Lauritzen, G. M. Rubin, D. D. Bock, *et al.*, *Neuron* **108**, 145 (2020).
- [16] S. S. Kim, H. Rouault, S. Druckmann, and V. Jayaraman, *Science* **356**, 849 (2017).
- [17] This formula shows that the metric can change signature

when the stability condition is violated. However, such a transition is not meaningful for a Riemannian metric, and likely indicates the collapse of the memory manifold.

- [18] J. I. Gold and M. N. Shadlen, *Annu. Rev. Neurosci.* **30**, 535 (2007).
- [19] B. W. Brunton, M. M. Botvinick, and C. D. Brody, *Science* **340**, 95 (2013).
- [20] E. C. Tolman, *Psychological review* **55**, 189 (1948).
- [21] E. H. Nieh, M. Schottdorf, N. W. Freeman, R. J. Low, S. Lewallen, S. A. Koay, L. Pinto, J. L. Gauthier, C. D. Brody, and D. W. Tank, *Nature*, 1 (2021).
- [22] The positive bias in this case is a consequence of initial conditions. The persistence of a finite fraction of the initial bias in the mean of h is an indication of the emerging slow manifold.
- [23] T. Can, K. Krishnamurthy, and D. J. Schwab, arXiv preprint arXiv:2002.00025 (2020).